Society For Biomaterials

Fabrication of cancellous biomimetic chitosan-based nanocomposite scaffolds applying a combinational method for bone tissue engineering

Zahra Jamalpoor,[1] Hamid Mirzadeh,[1,2,3] Mohammad Taghi Joghataei,[1,2] Darya Zeini,[3] Shadab Bagheri-Khoulenjani,[3] Mohammad Reza Nourani[4]

[1]Department of Tissue Engineering and Regenerative Medicine, Faculty of Advanced Technologies in Medicine, Iran University of Medical Sciences (IUMS), P.O. Box 1449614535, Tehran, Iran
[2]Cellular and Molecular Medical Research Center, Iran University of Medical Science, P.O. Box 1449614535, Tehran, Iran
[3]Polymer Engineering Department, Amirkabir University of Technology, P.O. Box 15875/4413, Tehran, Iran
[4]Tissue Engineering Division, Biotechnology Research Center, Baqiyatallah University of Medical Sciences, P.O. Box 14359-44711, Tehran, Iran

Received 26 July 2014; revised 23 August 2014; accepted 3 September 2014
Published online 00 Month 2014 in Wiley Online Library (wileyonlinelibrary.com). DOI: 10.1002/jbm.a.35320

Abstract: The aim of this study was to mimic the specific structure of bone and fabricate a biomimetic nano-hydroxyapatite (HA)/chitosan (Cs)/gelatin scaffolds using combination of particle leaching and freeze drying methods eliminating mold effects. To achieve an optimum structure, scaffolds with different gelatin/Cs weight ratio were fabricated. Morphological characterization of scaffolds by scanning electron microscopy method showed highly interconnected porous structures similar to cancellous bone with mean pore size ranging from 140 to 190 μm. Nano-HA crystals were dispersed homogeneously in the polymer matrix according to the energy-dispersive X-ray spectroscopy and transmission electron microscopy images. Fourier transform infrared and X-ray diffraction results disclosed that chemical interactions were formed between nano-HA, Cs, gelatin and crystallinity of each material decreased with blending. It was found that increasing the gelatin content significantly improved water uptake, degradation rate as well as attachment, infiltration and proliferation of Saos2 cells to the scaffolds. The presented results confirm that the designed biomimetic nano-HA /Cs/gelatin scaffolds can be used as promising substitutes for bone tissue engineering. © 2014 Wiley Periodicals, Inc. J Biomed Mater Res Part A: 00A:000–000, 2014.

Key Words: bone tissue engineering, nano-hydroxyapatite, chitosan/gelatin, particle leaching, freeze drying

How to cite this article: Jamalpoor Z, Mirzadeh H, Joghataei MT, Zeini D, Bagheri-Khoulenjani S, Nourani MR. 2014. Fabrication of cancellous biomimetic chitosan-based nanocomposite scaffolds applying a combinational method for bone tissue engineering. J Biomed Mater Res Part A 2014:00A:000–000.

INTRODUCTION

Millions of people worldwide suffer from bone defects needing treatment each year. The main concerns of current treatments (i.e., autografts, allografts, and xenografts) are donor site morbidity and shortages,[1] the risk of immunogenic rejection and disease transmission.[2] These shortcomings have led to extensive research in bone tissue engineering (BTE) as a promising alternative method to bone grafting. In BTE approach, three required components, namely bone forming cells, porous and biodegradable scaffolds and growth factors, to integrate with each other to achieve optimal bone regeneration.[3,4] Scaffolds, as an artificial matrix, provide the necessary physicochemical support for cell attachment, proliferation, and differentiation. In addition, they guide bone regeneration and are replaced gradually with new bone tissue.[5] Thus, material properties and right design of the scaffold are essential in determining desired cellular responses.[6,7] Recently, natural polymers and their composites have been used more than other materials in BTE.[8,9] Biopolymers are highly organized structures containing ligands that can bind to cell receptors and guide cellular function at various stages of growth and development. Chitosan (Cs) is a linear polysaccharide derived from partial de-acetylation of chitin. Because of its similarity to glycosaminoglycans, it plays a key role in regulating cell behavior.[10] Cs is considered an effective biomaterial for tissue engineering applications because of many excellent properties such as antibacterial activity, nontoxicity, and hemostatic effect.[11,12] Blending of Cs with other natural polymers and bioceramics can improve both its biological and mechanical properties.[5,13] Gelatin (Gel) is the denatured form of collagen with no antigenicity and low cost.[14] The formation of the polyelectrolyte complex with Cs as well as the presence of Arg-Gly-Asp (RGD)-like sequences in Gel, mimics the organic phase of natural bone extracellular matrix (ECM), improving cell attachment and activity.[15,16]

Correspondence to: H. Mirzadeh; e-mail: Mirzadeh@aut.ac.ir and M. T. Joghataei; e-mail: Joghataei@iut.ac.ir
Contract grant sponsor: Iran National Science Foundation (INSF); contract grant number: 92002917

TABLE I. The Original Amount and Weight Ratios of the Scaffolds Components for the Preparation of nHA/Cs/Gel Scaffolds

Sample Code	Biopolymer Concentration (g/mL)	Gel/Cs (wt/wt)	nHA/polymer (wt/wt)	NaCl/ polymer (wt/wt)
2	0.06	2	0.25	10
1	0.04	1	0.25	10
0.5	0.03	0.5	0.25	10

Hydroxyapatite (HA) is the major mineral constituent of native bone and is an attractive bioceramic for BTE because of its excellent osteoconductivity, nonimmunogenicity, and bioactivity.[17] Thus, the inclusion of HA nanoparticles (nHA) into the polymeric matrix not only mimics the structure of bone, but also improves both biological activity and mechanical strength of scaffolds.[9,18] The processing method must allow the fabrication of three-dimensional (3D) scaffolds with optimum porosity and pore sizes, as well as bone matching mechanical strength and suitable cell responses.[19] Different methods have been used to prepare 3D scaffold, including particle leaching,[20] gas forming,[21] 3D printing,[22] selective laser sintering,[23] freeze drying,[24] among others. To create scaffolds with improved microarchitecture, a combination of particle leaching with other techniques, such as freeze drying can be useful.[25–27] The objective of this study was to develop a biomimetic nHA/Cs/Gel scaffold by a combination of particle leaching and freeze drying methods. To achieve an optimum structure, mold effect was eliminated during the freeze drying process and different scaffolds were prepared by changing gelatin/Cs weight ratio. The designed scaffolds were characterized for their structural, physicochemical, and biological properties.

MATERIALS AND METHODS

Materials

High molecular weight Cs, nanosize HA (<200 nm), *N*-(3-Dimethylaminopropyl)-*N*′-ethylcarbodiimide hydrochloride (EDC), RPMI-1640, and (3-(4,5-dimethylthiazol-2-yl)-2,5-diphenyltetrazolium bromide (MTT) were purchased from Sigma-Aldrich (USA). Gelatin powder (microbiology), acetic acid, and sodium chloride (NaCl) were obtained from Merck (Germany). Penicillin-streptomycin (10,000 IU to 10,000 μg/mL), 0.25% trypsin-EDTA, fetal bovine serum (FBS), and phosphate buffer saline (PBS) were purchased from GIBCO, Invitrogen Corporation. Other reagents used were of an analytical or cell culture grade.

Scaffold fabrication

Three types of porous nHA/Cs/Gel composite scaffolds with different weight ratios of Gel to Cs were produced by a combination of particle leaching and freeze drying methods using NaCl as porogen (Table I). To synthesize the scaffolds, a certain amount of nHA powder was suspended into 1% v/v acetic acid solution. The mixture was stirred at room temperature for 30 min and treated by ultrasonication for 60 s. Then, Cs was introduced into the nHA suspension under agitation and the nHA/Cs mixture was stirred overnight. Afterward, gel powder was added and stirred for 12 h at 40°C. Next, NaCl crystals were added and mechanically stirred for 48 h in water bath at 40°C. The resulting product was poured into Teflon molds, uniformly packed and air dried. The dried samples were crosslinked by immersion into 50 m*M* EDC solution in acetone–water mixture (9:1 v/v) and slowly shaken for 48 h. Subsequently, the scaffolds were treated with 100% ethanol solution for 20 min to neutralize acetic acid and salt particles were extracted by deionized water for 7 days at a low shaking rate. The desalted scaffolds were freeze dried for 48 h and the final scaffolds were stored in a dry place until use.

Scaffold characterization

Structural morphology. Scanning electron microscopy (SEM, II XMU Tescan, Czech Republic) with qualitative energy-dispersive X-ray spectroscopy (EDX) capabilities was used to assess structural morphology and to verify calcium and phosphorus presence and distribution. nHA particles dispersion into the polymeric matrix was examined by a Phillips transmission electron microscopy (TEM) with 20 kV acceleration voltage. The mean pore size was estimated from SEM micrographs. At least 200 pores were assessed from different areas of each sample.

Chemical characterization. Scaffolds were chemically characterized by Fourier transform infrared spectroscopy, FTIR (Bruker Equinox 55, Germany) and X-ray diffraction, XRD (Siemens D-500, USA) techniques.

Water uptake studies. Scaffolds were immersed into 37°C PBS buffer solution (pH 7.4) while shaking at 60 rpm. To evaluate water uptake ability at predetermined time intervals, samples were weighed after removing excess water and water uptake ability (E_A) was calculated using the following equation:

$$E_A = [(W_w - W_d)/W_d] \times 100$$

where W_w and W_d are the wet and initial dry weights of scaffold, respectively.

In vitro biodegradation test

Scaffolds were presoaked in a PBS solution (pH 7.4) containing 10,000 U/mL lysozyme, withdrawn at regular time intervals, washed with deionised water, and dried at 40°C by an oven. The degradation rate (D) was calculated as follows:

$$D = [(W_d - W_t)/W_d] \times 100$$

where W_d is the initial dry weight and W_t is the weight at time t.

Porosity measurement. The porosity of nanocomposite scaffolds was measured by liquid displacement method [25] using the following formula:

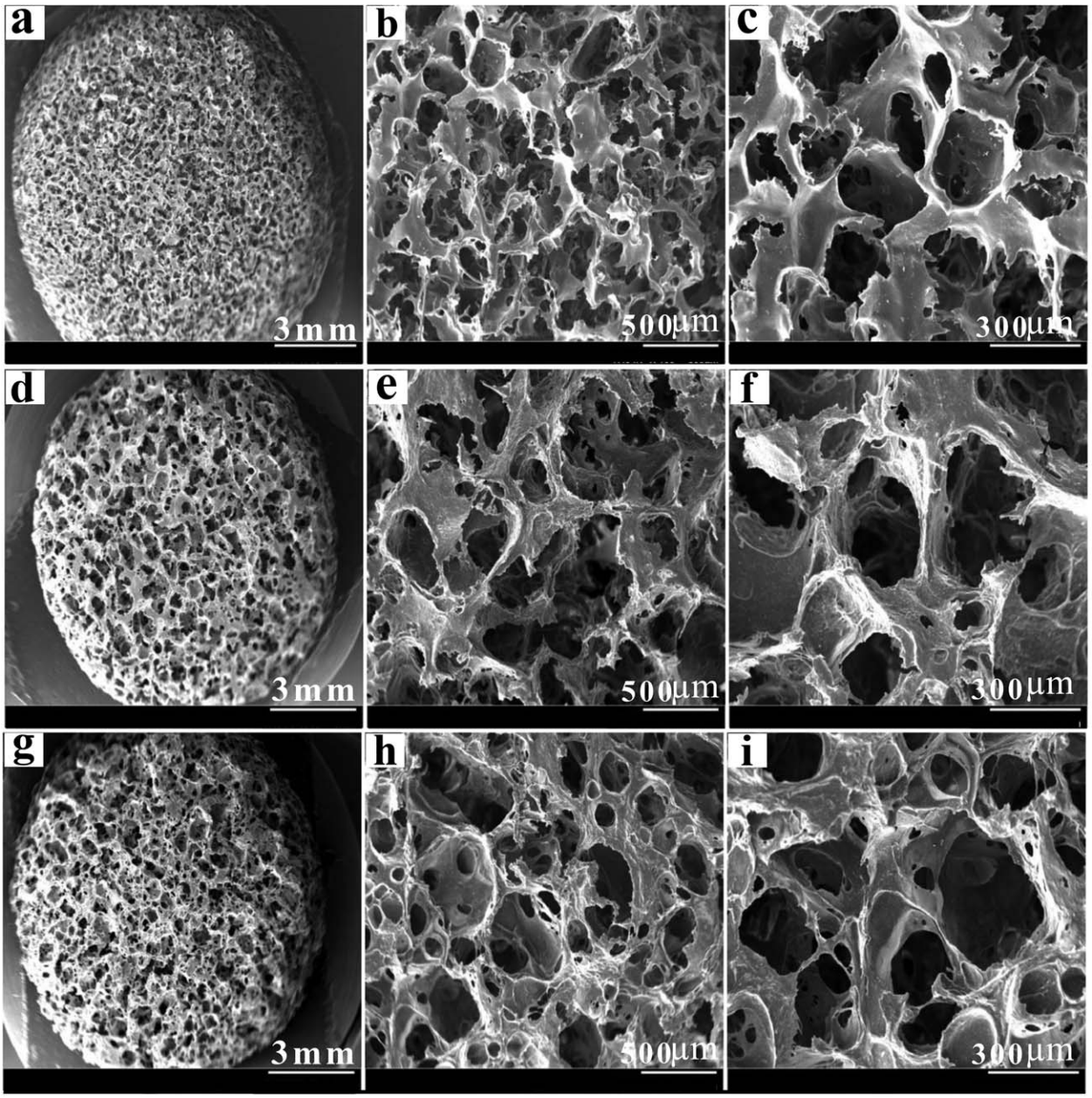

FIGURE 1. SEM micrographs at three different magnification of the surface of nHA/Cs/Gel scaffolds prepared by the combination of particle leaching and freeze drying methods. (a–c) Sample 2, (d–f) sample1, and (g–i) sample 0.5.

$$\text{Porosity} = [(W_w - W_d)/(W_w - W_1)] \times 100$$

where W_w is the wet weight of sample after being taken out from ethanol, W_d is the dry weight of sample, and W_1 is the weight of sample in ethanol.

Mechanical property. The compressive strength and modulus of the scaffolds in dry state were measured by mechanical testing machine (SANTAM, STM-20), fitted with a 1-kN load cell. The dimensions of samples were 10 × 10 × 6 mm^3, where 6 was the thickness. The cross-head speed was set at 1 mm/min, and load was applied until 60% reduction in original thickness was achieved. The elastic modulus (E) was determined as the initial linear section of the stress-strain curve.

In vitro cell culture studies

Cell culture and seeding. Human Osteogenic Sarcoma (Saos-2) cells were cultured in flasks with RPMI-1640 supplemented by 10% FBS and 1% penicillin/streptomycin in a humidified incubator at 37°C with 5% CO_2 and 95% air. When the cells reached 80% confluence, they were harvested from flasks using 0.25 trypsin-EDTA, re-suspended, calculated, and used for seeding onto the scaffolds. Prewetted sterilized scaffolds with dimensions of 9 × 9 × 2 mm^3 were placed in 24-well culture plates. A 50-μL cell suspension containing approximately 25,000 cells

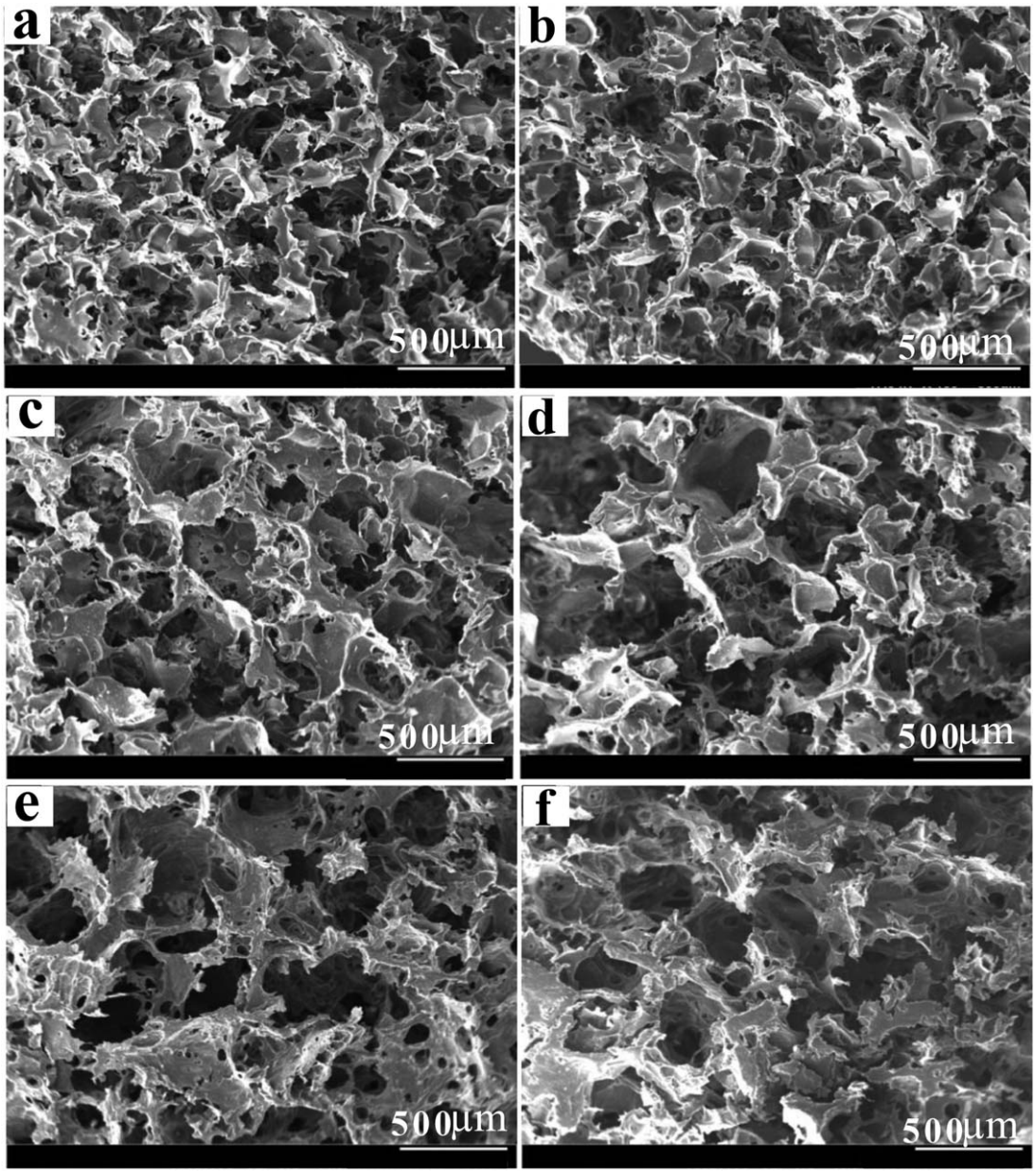

FIGURE 2. SEM micrographs of the sectional morphology (horizontal and vertical) of the nHA/Cs/Gel scaffolds. (a, c, e) horizontal and (b, d, f) vertical sections of sample 2, 1, and 0.5, respectively.

were uniformly seeded drop-wise on top of the scaffold in each well. Cell-seeded scaffolds were incubated for 3 h at 37°C to allow the cells to adhere. Next, an additional 200 μL of culture medium was added into each well and incubation was resumed. The medium was changed every day for 7 days.

Cell seeding efficacy and cytotoxicity tests. Initial cell-seeding efficiency (CSE) was determined by a method previously published.[28] Initial cell adhesion was calculated after 6 h as follows:

$$(\text{CSE})\ (\%) = [(N_i - N_u)/N_i] \times 100$$

where N_i is the initial cell number and N_u is the number of cells unattached to the scaffold

The cytotoxicity of nHA/Cs/Gel scaffolds was examined by observing the behavior of cells in the vicinity of scaffolds 3 days after cell seeding using inverted microscope.

Cell morphology and localization. The morphology of attached Saos-2 cells within the scaffolds was studied using SEM after 3 days of cell seeding. Cell-seeded scaffolds were fixed in 2.5% glutaraldehyde overnight, then washed with PBS, dehydrated in a graded series of ethanol (50–100%), and dried in freeze drier overnight. The cell localization and distribution within the scaffolds were observed using fluorescence microscopy after staining with DAPI (5 μL/mL) dye for 5 min at room temperature.

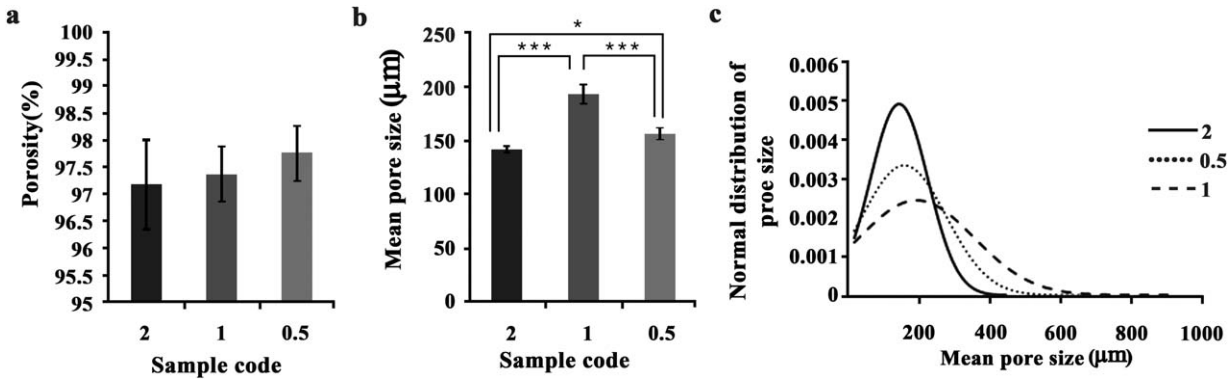

FIGURE 3. Morphological properties of nHA/Cs/Gel scaffolds. (a) prosity, (b) pore size, and (c) normal distribution of pore size.*$p < 0.05$, ***$p < 0.001$.

Proliferation test. Cellularity of Saos-2 cells onto the scaffolds was examined by MTT test. The medium was removed 1, 3, 5, and 7 days after cell seeding and fresh medium containing MTT (5 mg/mL in PBS) was added into each well followed by incubation for 4 h in the dark. Then, dimethyl sulfoxide was used to dissolve formazan crystals. Optical densities (OD) of solution were measured at 570 nm.

Statistical analysis

All results are presented as the mean ± standard error of mean. A one-way analysis of variance (ANOVA) followed by Newman-Kules post-test was performed to determine the effect of Gel to Cs ratio on pore size, porosity, mechanical strength and modulus, and cell seeding efficacy. A two-way ANOVA followed by Bonferroni post-test was used to analyze swelling ratio, degradation, and cell proliferation. A value of $p < 0.05$ was considered to be statistically significant.

RESULTS AND DISCUSSIONS

Scaffold morphology

In this current study, we combined particle leaching with freeze drying method to avoid formation of a dense surface impeding penetration of seeded cells—a drawback of using freeze drying alone.[29] Figures 1 and 2 demonstrate that prepared scaffolds were highly porous and formed interconnected networks mimicking the structure of cancellous bone. Porosity of scaffolds was equal or greater than 97% [Fig. 3(a)]. A porous surface can facilitate mechanical interlocking between the scaffold and the surrounding tissue to enhance mechanical stability of the implanted scaffold [30] and to improve cell adhesion by increasing the surface area.[31] The open and interconnected pores promote gas and nutrient transport, which is vital for cell proliferation, differentiation,[32] migration,[33] revascularization,[34] and new bone formation.[35] Range of pore size for sample 0.5, 1, and 2 was 15–670, 17–920, and 16–440 μm, respectively. The mean

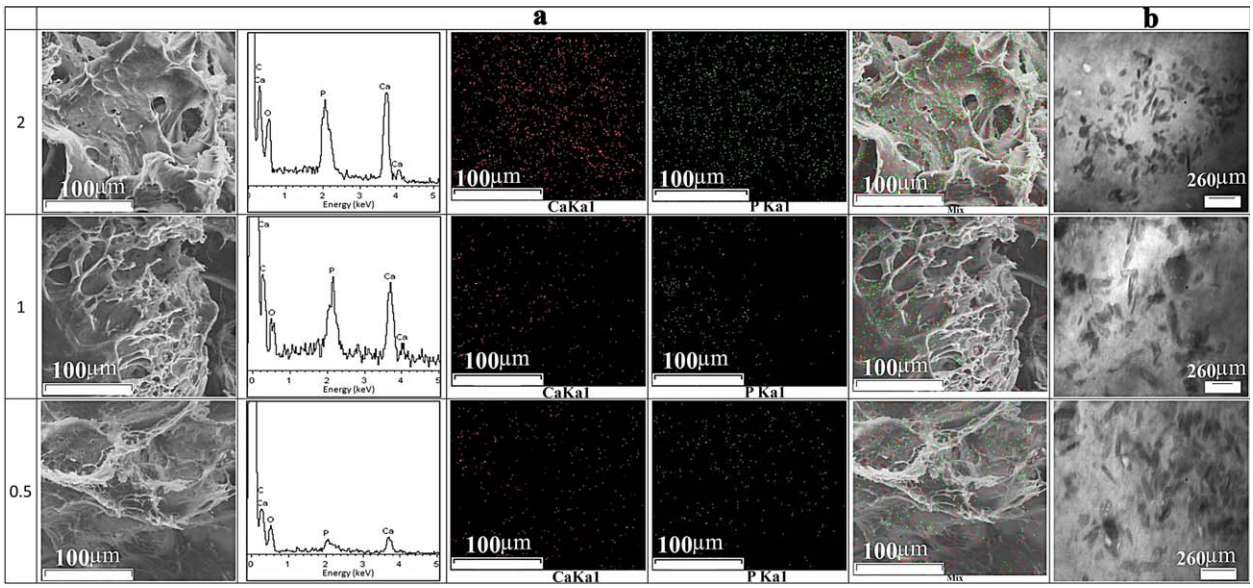

FIGURE 4. (a) SEM/EDX images with element mapping analysis of nHA/Cs/Gel scaffolds. (b) TEM micrographs of dispersion of nHA in Gel/Cs matrix. [Color figure can be viewed in the online issue, which is available at wileyonlinelibrary.com.]

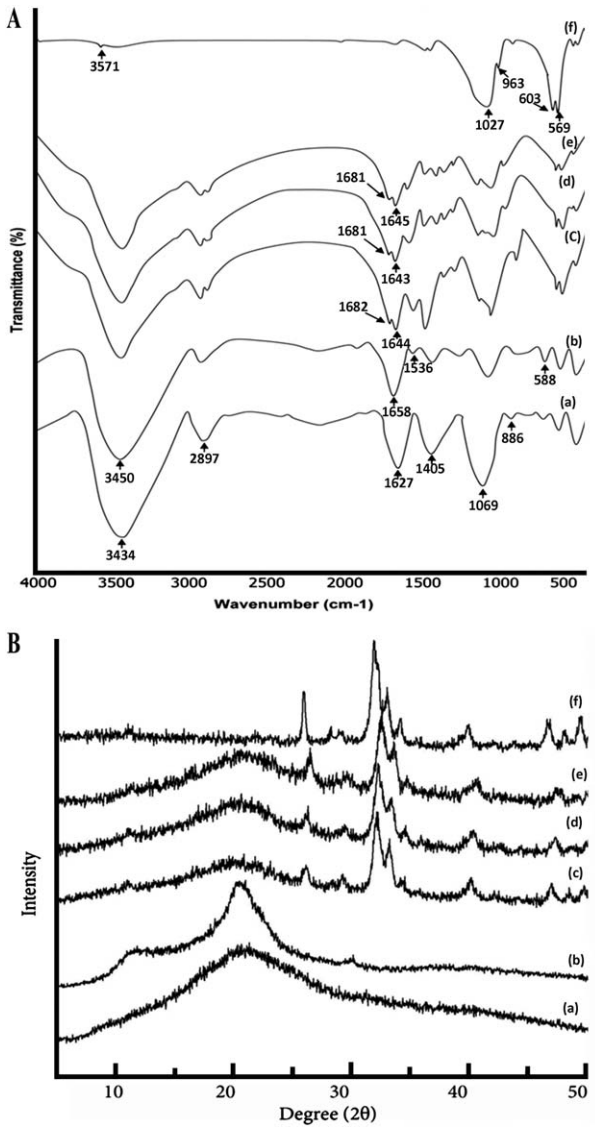

FIGURE 5. (A) FTIR spectra and (B) XRD patterns of nHA/Cs/Gel scaffolds. (a) pure Cs, (b) pure Gel, (c) sample 2, (d) sample 1, (e) sample 0.5, (f) nHA.

pore size was significantly different between these groups. It was remarkably larger in sample 1 compared with others ($p < 0.001$) [Fig. 3(b)]. However, pore size distribution in sample 2 was more homogenous than sample 0.5 and 1 [Fig. 3(c)]. It seems the changes in pore size are attributed to the freeze drying process. During thermal phase separation in freeze-drying process, absorbed water molecules in hydrogels move out and form some ice crystals. The higher the swelling ratio, the higher the water content in the scaffolds, leaving larger ice crystals behind. Because gel is more hydrophilic than Cs, it is believed that increasing gel in scaffold would enhance water absorption.[36] Increase in pore size by increasing gel/Cs ratio from 0.5 to 1 can be attributed to increase in swelling ratio of samples. However, an unexpected decrease in pore size by further increase in gel/Cs ratio, from 1 to 2, is explainable by changes in crosslinking density of scaffolds. Any increase in gel/Cs ratio means increment of COOH functional groups in the polymeric matrix. Crosslinking of Cs-gel using EDC happens via interaction of COOH (present in gel chains) and NH_2 groups (present in both Cs and gel chains) forming an amide bond. Higher gel/Cs ratio could result in higher crosslinking density. Any rise in crosslinking density results in lesser mobility of polymeric chains during the freezing process [27] and therefore reduces water penetration into the growing nucleus. This whole process prevents the formation of large ice crystals during the freeze drying step.[25,37] Observing various sections in the fabricated scaffolds, majority of pores were round. Using mold in the freeze drying step usually results in heat transfer variation between the air-exposed surface of the scaffold and other sides, attributing to different pore shapes. Alizadeh et al.[27] used a Wilton mold during the freeze drying step, which imposed a binary morphology in the vertical section of their scaffolds. Pores exposed to air were side-oriented, whereas others in contact with the mold were columnar. As they reported, both side-oriented and columnar pores had lower interconnectivity. In this current research, to eliminate the mold effect, we benefited from a piece of screen mesh mounted on a container, on which the scaffolds were laid (after taking it out of water and immediately before freeze drying). Fully air-circulated samples during freeze drying ensured a uniform heat transfer across all surfaces and diminished the pore shape variation to a great extent. When a porous structure is prepared by the combination method, pore formation occurs during two equally named steps. In particle leaching step, supersaturated NaCl particles were precipitated, recrystallized, and washed away to yield macropores.[25,26] The micropores

TABLE II. Assignment of FTIR Spectra of nHA/Cs/Gel Scaffolds in Fig. 4A

IR Absorption Band (cm^{-1})	Cs	Gel	nHA	Sample 2	Sample 1	Sample 0.5
3571	—	—	—O—H	—O—H	—O—H	—O—H
3450-343	—N—H	—N—H	—	—N—H	—N—H	—N—H
1658	—	—C(=O)	—	—C(=O)	—C(=O)	—C(=O)
1627	Amidel	—	—	Amidel (1644)	Amidel (1643)	Amidel (1645)
1536	—	Amide II	—	Amide II	Amide II	Amide II
1405	—C—H	—	—	—C—H	—C—H	—C—H
1069	—C—O	—	—	—C—O	—C—O	—C—O
1027	—	—	—P=O	—P=O (1018)	—P=O (1017)	—P=O (1015)
963	—	—	P(=O)	P(=O) (955)	P(=O) (953)	P(=O) (954)
603	—	—	P(=O)	P(=O) (580)	P(=O) (578)	P(=O) (576)
569	—	—	P(=O)	P(=O) (557)	P(=O) (555)	P(=O) (556)

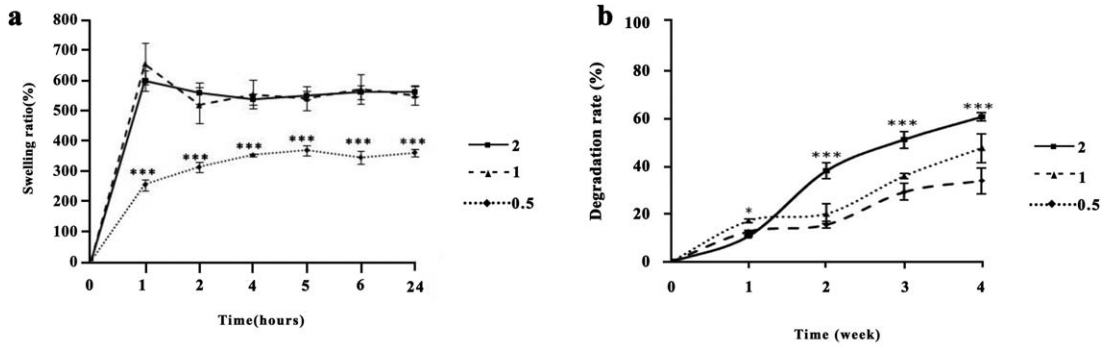

FIGURE 6. (a) Water uptake ability and (b) degradation rate of nHA/Cs/Gel scaffolds. $*p < 0.05$, $***p < 0.001$ compared with other groups, $n = 5$.

formed within the thin wall of the polymer during the freeze drying step, increasing porosity and interconnectivity.[25] However, such high NaCl concentration rises the risk of precipitation, resulting in heterogeneous patterns of porosity.[26,27] Despite the salt to polymer weight ratio of 10, in this study, the pores were distributed uniformly along the whole thickness of scaffolds. To ensure such uniformity, the salt/polymer mixture was mechanically stirred at least 48 h in a 45°C water bath. Gradual evaporation of the solvent during the stirring period rendered the mixture thicker and thus less precipitative. EDX analysis revealed the presence of calcium and phosphate in all three samples [Fig. 4(a)]. In addition, the uniform distribution of the inorganic substances was unveiled by elemental mapping analysis. The source of calcium and phosphate is attributed to nHA particles that homogeneously dispersed into the polymeric matrix without any sort of agglomeration [Fig. 4(b)].

FTIR. The assignment of peaks in FTIR spectra of Cs, Gel, nHA, and nHA/Cs/gel nanocomposite scaffolds [Fig. 5(a)] are summarized in Table II. Accordingly, all characteristic bands in pure materials are present in the nanocomposites. The FTIR spectra of nanocomposites show that the amide I peak at 1627 cm^{-1} in Cs and carboxyl peak at 1658 cm^{-1} in gel shift to higher wave number (red shift) at 1644 and 1682 cm^{-1}, respectively. This may be related to the formation of hydrogen bond between Cs and gel molecules.[16,38] In addition, phosphate group peaks move to lower wave number, which can be attributed to electrostatic or polar interaction between carboxyl groups of gel and/or C═O groups of Ch with Ca^{2+} as well as amino groups of Cs and gel with phosphate of nHA.[16,18]

XRD. Figure 5(b) shows the XRD diffraction patterns of pure Cs, Gel, nHA, and nHA/Cs/gel nanocomposites. Both Cs and Gel are characterized by one crystalline peak at $2\theta = 20.9°$ and 20.5°, respectively.[38] nHA has diffraction peaks at $2\theta = 25.7°$, 26.3°, 29.1°, 32.3°, 39.6°, and 40.8°.[18] In nanocomposites, the crystalline peaks of Cs and gel merged together and became significantly weaker than pure Cs and gel. XRD data indicate that the degree of cryatallinity decreased with nanocomposite formation. This can be related to chemical interaction between polymer matrix and nanoparticles, in line with FTIR data.

Water uptake. A remarkable property of scaffold evaluation in tissue engineering is their capacity to absorb water. It facilitates nutrient and metabolic products transport as well as cell infiltration into the construct. In addition, water uptake accelerates internal surface area via increasing pore size and porosity.[18] As shown in Figure 6(a), all samples absorbed water at least three times their initial weight when immersed into PBS. By increasing gel/Cs weight ratio from 0.5 to 1, water uptake at equilibrium increased

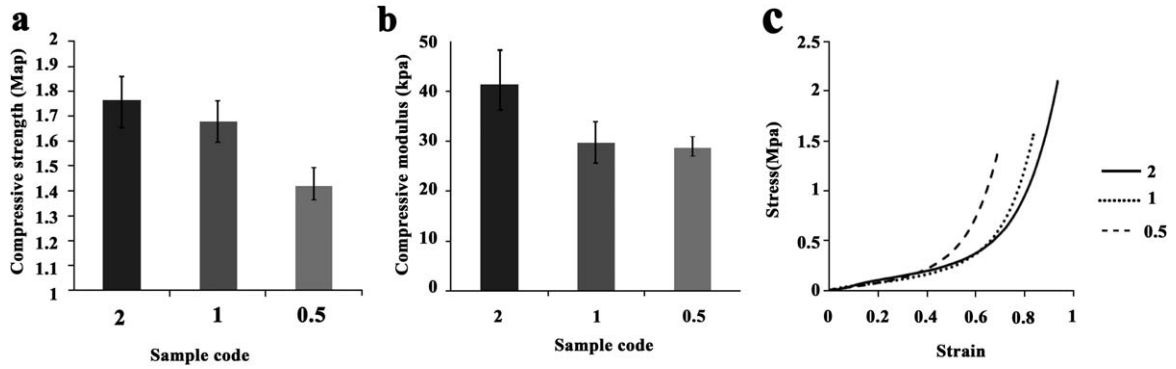

FIGURE 7. Mechanical properties of nHA/Cs/gel scaffolds. (a) Compressive strength, (b) compressive modulus, and (c) stress–strain curve, $n = 5$.

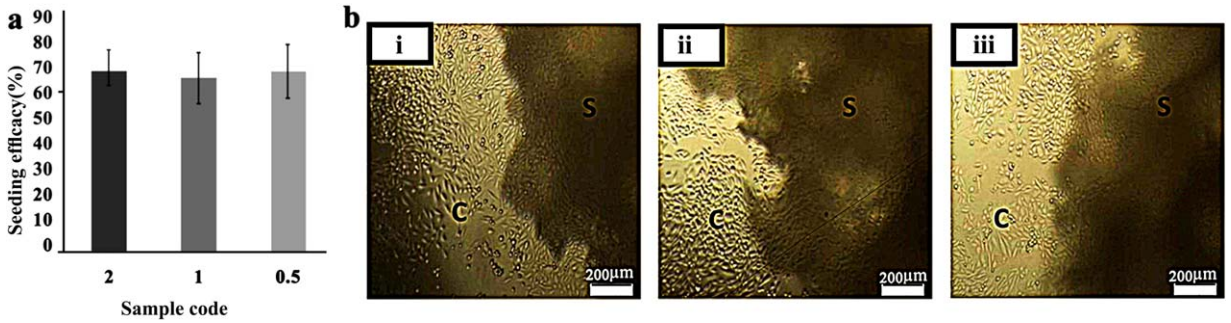

FIGURE 8. (a) Seeding efficacy and (b) inverted microscope images of Sao2s cells (denoted as C) adjacent to nHA/Cs/Gel scaffolds (denoted as S) after 3 days. (i) sample 2, (ii) sample 1, and (iii) sample 0.5. [Color figure can be viewed in the online issue, which is available at wileyonlinelibrary.com.]

significantly from 300 to 600%. Further increase in gel/Cs weight ratio did not affect the water uptake ability. The kinetic of water uptake demonstrates that the samples 2 and 1 reached their maximum absorption after just 1 h (i.e., 596 and 625%, respectively). However, it took sample 0.5 five hours to swell by 366%. Less hydrophilicity of Cs, compared with gel, may account for this result.[39] The water uptake of sample 2 and 1 was significantly greater than sample 0.5 at all time points ($p < 0.001$). The higher water absorption in samples 2 and 1 is due to the greater hydrophilicity of gelatin polymer.[6] Considering the previous statements, one expects to observe more water absorption in sample 2 than sample 1 because it has more gel, yet the difference was not significant. Stronger crosslinking in sample 2 possibly did not allow it to absorb as much as sample 1. On the other hand, larger pore size in sample 1 would further enhance water absorption exceeding that of sample 2 in maximum water uptake.

Degradation rate. To assess the degradation behavior of nHA/Cs/gel scaffolds, lysozyme enzymatic solution was used. The biodegradation percentage for sample 2, 1, and 0.5 was 61, 48, and 34%, respectively, at the end of week 4 [Fig. 6(b)]. Our results indicate that biodegradation speeded up with any increase in gel concentration. This implies the higher hydrophilicity of gel lead to faster hydrolysis of the polymeric chain, which is consistent with other reports.[27,38,39] The kinetic of biodegradation rate revealed that sample 1 decomposed significantly quicker at the end of the first week, despite lower gelatin content ($p < 0.001$). It seems that enzyme penetration into sample 1 was enhanced by larger pore size, but impeded in sample 2 by

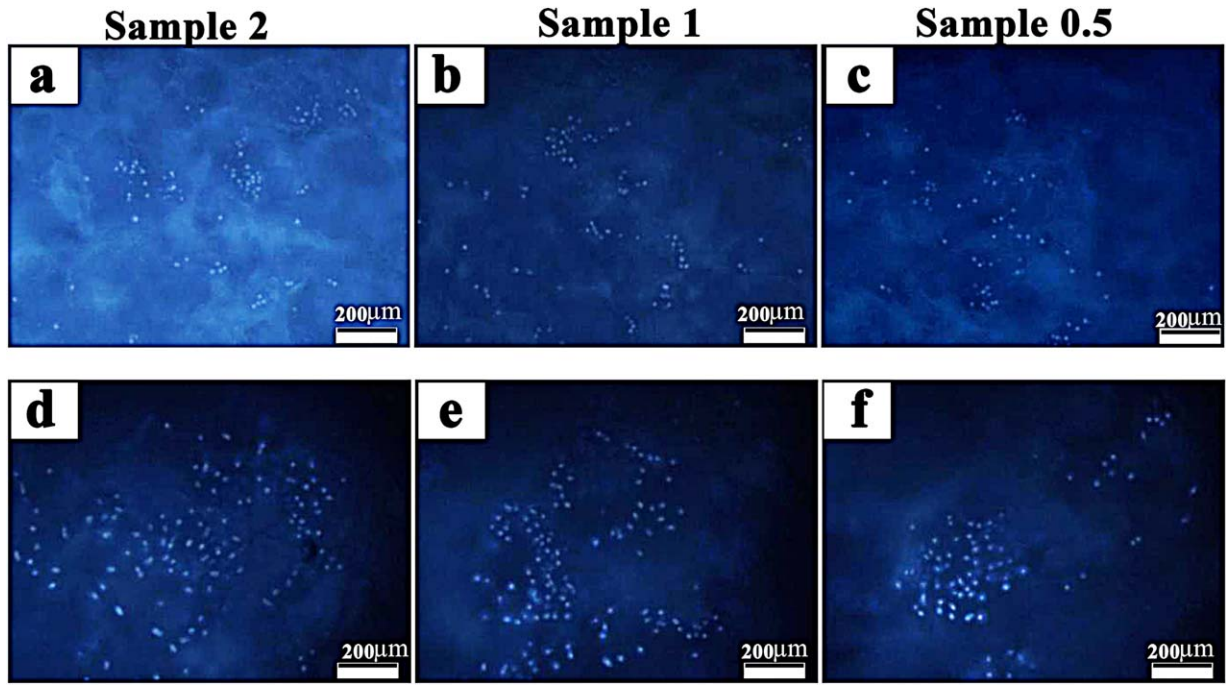

FIGURE 9. Fluorescence microscopy images of cell-seeded nHA/Cs/gel scaffolds (a, b, c) 6 h and (d, e, f) 3 days after staining with DAPI nuclei staining dye. [Color figure can be viewed in the online issue, which is available at wileyonlinelibrary.com.]

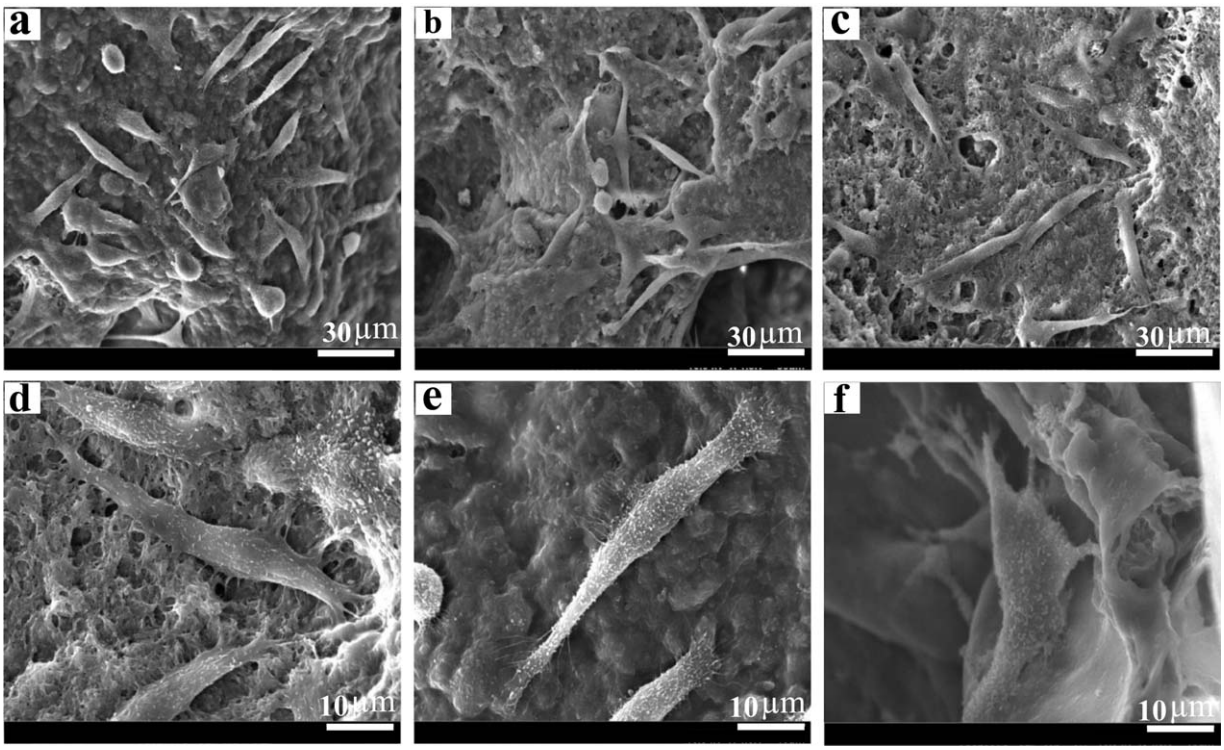

FIGURE 10. SEM micrographs of cell-seeded nHA/Cs/gel scaffolds. (a, d) sample 2, (b, e) sample 1, and (c, f) sample 0.5.

stronger crosslinking in the first week. Once crosslinking subsides, more gelatin accounts for the degradation rise. Compared with other reports, the water uptake and degradation rate was relatively less in our samples,[38,40] which could be attributed to the presence of nHA.[5,18]

Mechanical properties. nHA/Cs/Gel scaffolds were tested for compressive properties in dry state. As displayed in Figure 7, compressive strength of samples 2, 1, and 0.5 were 1.75, 1.67, and 1.42 MPa, respectively, within the range of human trabecular bone (i.e., 1–10 MPa),[28] and were increased by augmenting the gel content. In addition, compressive modulus and strength as well as stress and strain range in sample 2 were more than other samples, although not significant. As mentioned in the FTIR section, the crosslinking effect of EDC increases with rise in gel content leading to mechanical strengths enhancement.[40] This effect is strong enough to override the similar but smaller effect of Cs on mechanical strength.[39] In other words, sample 2 had the highest compressive strength of all.

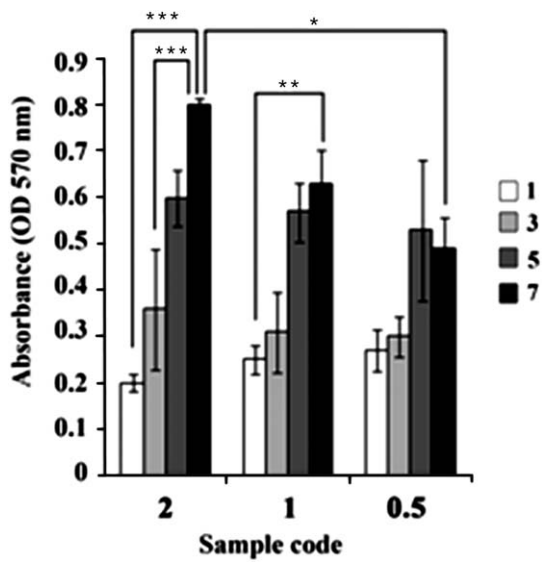

FIGURE 11. MTT proliferation test of Sao_2s cells on nHA/Cs/Gel scaffolds. $*p < 0.05$, $**p < 0.01$, $***p < 0.001$, $n = 5$.

In vitro biological studies

Cell seeding efficacy. The initial cell seeding efficacy in all three scaffolds was more than 70% and there was not any notable difference between the three groups (Fig. 8). Amini et al.[28] showed that the cell seeding efficacy decreases with increase in porosity. It seems that in our study equal porosity between the three types of scaffolds has inhibited variation in cell seeding efficacy.

Cell morphology. SEM micrographs of cell-seeded scaffolds on day 3 are illustrated in Figure 9. They helped to clarify the interaction between Saos-2 cells and nHA/Cs/gel matrices. Cell adhesion is well supported in all three samples as the cells spread on the surface of the scaffolds and exhibit fibroblast-like morphology. Higher magnification of the micrographs [Fig. 9(d–f)] unveiled the extensive cytoplasmic

processes and filopodia as anchoring points of cells to the surfaces.

Cell localization and distribution. To evaluate cell localization and distribution, cell-seeded scaffolds were viewed by fluorescent microscopy after staining with DAPI dye. As shown in (Fig. 10), 6 h after seeding, the cell number was equal in all samples, consistent with the seeding efficacy results. After 3 days, cells were distributed within the scaffolds and almost attached to the pore walls. In addition, the number of cells in samples 1 and 2 were higher than in sample 0.5, implying more cytocompatibility with higher gel content.[38] Cells adhere to ECM proteins such as fibronection via integrin molecules when integrin connect to ligand. The presence of NH3 and COOH functional groups in Cs and gel facilitate cell–polymer interaction. This interaction apparently improved cell attachment and proliferation.[41,42]

Cell proliferation. MTT test was used to evaluate cell proliferation in all specimens. Results revealed that both Gel content and culture duration affect cell proliferation (Fig. 11). Sample 2 had the highest proliferation rate on day 7, which was statistically significant when compared to sample 0.5 ($p < 0.05$), but not sample 1. The assessment of proliferation rate profile of sample 1 and 2 showed that OD absorbance on days 5 and 7 were significantly higher than those obtained on day 1 ($p < 0.01$ and $p < 0.001$, respectively). Moreover, in sample 2, OD absorbance was higher on day 7 compared with day 3 ($p < 0.001$). The degree of cell proliferation on nHA/Cs/Gel scaffolds was different despite their similar porosity and interconnectivity. It seems that the gel is a more suitable substrate for cell attachment, proliferation, and differentiation because of the presence of RGD sequences similar to collagen. Thus, greater amount of gel can facilitate cellular activity.[13,38] As presented in MTT results, there was no significant difference in cell proliferation rate between sample 1 and 2 despite the lower gel in sample 1. It seems the larger pore size in sample 1 promoted nutrient absorption from the culture medium, advancing the growth.

CONCLUSION

In this study, we successfully synthesized biomimetic highly porous nHA/Cs/gel scaffolds by combining particle leaching and freeze drying methods and characterized them by different analytical tests. All scaffolds fabricated by this method had cancellous bone like microstructure with open and interconnected pores both on the surface and within the scaffolds. Accordingly, we claim the procedure used could eliminate the main problem associated with freeze drying technique, that is, non-open pores on the surface of the scaffold. The scaffolds also possessed suitable water absorption and biodegradation rate as well as mechanical strength, influenced significantly by gelatin to Cs ratio. Saos-2 cells could well attach, spread, and infiltrate into the scaffolds properly. Gelatin-to-Cs ratio and pore size were two main factors determining the degree of proliferation. This study suggests that nHA/Cs/Gel scaffolds prepared by the combination of particle leaching and freeze drying can be a promising substitute for BTE applications.

ACKNOWLEDGMENTS

The research was financially supported by Iran National Science Foundation (INSF) through research Grant No. 92002917.

REFERENCES

1. Mauffrey C, Madsen M, Bowles RJ, Seligson D. Bone graft harvest site options in orthopaedic trauma: A prospective in vivo quantification study. Injury 2012;43:323–326.
2. Paderni S, Terzi S, Amendola L. Major bone defect treatment with an osteoconductive bone substitute. Chir Organi Mov 2009;93:89–96.
3. Langer RS, Vacanti JP. Tissue engineering: the challenges ahead. Sci Am 1999;280:86–89.
4. Chen Q, Zhu C, Thouas G. Progress and challenges in biomaterials used for bone tissue engineering: Bioactive glasses and elastomeric composites. Prog Biomater 2012;1:1–22.
5. Thein-Han W, Misra R. Biomimetic chitosan—Nanohydroxyapatite composite scaffolds for bone tissue engineering. Acta Biomater 2009;5:1182–1197.
6. Loh QL, Choong C. Three-dimensional scaffolds for tissue engineering: Role of porosity and pore size. Tissue Eng Part B Rev 2013;19:485–502.
7. Tour G, Wendel M, Tcacencu I. Cell-derived matrix enhances osteogenic properties of hydroxyapatite. Tissue Eng Part A 2010; 17:127–137.
8. Costa-Pinto AR, Reis RL, Neves NM. Scaffolds based bone tissue engineering: The role of chitosan. Tissue Eng Part B Rev 2011;17: 331–347.
9. Swetha M, Sahithi K, Moorthi A, Srinivasan N, Ramasamy K, Selvamurugan N. Biocomposites containing natural polymers and hydroxyapatite for bone tissue engineering. Int J Biol Macromol 2010;47:1–4.
10. Nishikawa H, Ueno A, Nishikawa S, Kido JI, Ohishi M, Inoue H, Nagata T. Sulfated glycosaminoglycan synthesis and its regulation by transforming growth factor-β in rat clonal dental pulp cells. J Endod 2000;26:169–171.
11. Kim IY, Seo SJ, Moon HS, Yoo MK, Park IY, Kim BC, Cho CS. Chitosan and its derivatives for tissue engineering applications. Biotechnol Adv 2008;26:1–21.
12. Khor E, Lim LY. Implantable applications of chitin and chitosan. Biomaterials 2003;24:2339–2349.
13. Pezeshki-Modaress M, Rajabi-Zeleti S, Zandi M, Mirzadeh H, Sodeifi N, Nekookar A, Aghdami N. Cell-loaded gelatin/chitosan scaffolds fabricated by salt-leaching/lyophilization for skin tissue engineering: In vitro and in vivo study. J Biomed Mater Res Part A 2013; doi: 10.1002/jbm.a.35054.
14. Liu X, Smith LA, Hu J, Ma PX. Biomimetic nanofibrous gelatin/apatite composite scaffolds for bone tissue engineering. Biomaterials 2009;30:2252–2258.
15. Nandagiri VK, Gentile P, Chiono V, Tonda-Turo C, Matsiko A, Ramtoola Z, Montevecchi FM, Ciardelli G. Incorporation of PLGA nanoparticles into porous chitosan–gelatin scaffolds: Influence on the physical properties and cell behavior. J Mech Behav Biomed Mater 2011;4:1318–1327.
16. Li J, Chen Y, Yin Y, Yao F, Yao K. Modulation of nano-hydroxyapatite size via formation on chitosan–gelatin network film in situ. Biomaterials 2007;28:781–790.
17. Murugan R, Ramakrishna S. Bioresorbable composite bone paste using polysaccharide based nano hydroxyapatite. Biomaterials 2004;25:3829–3835.
18. Peter M, Ganesh N, Selvamurugan N, Nair S, Furuike T, Tamura H, Jayakumar R. Preparation and characterization of chitosan–gelatin/nanohydroxyapatite composite scaffolds for tissue engineering applications. Carbohydr Polym 2010;80:687–694.
19. Gomes ME, Godinho J, Tchalamov D, Cunha A, Reis R. Alternative tissue engineering scaffolds based on starch: Processing

methodologies, morphology, degradation and mechanical properties. Mater Sci Eng C 2002;20:19–26.
20. Ma PX. Scaffolds for tissue fabrication. Mater Today 2004;7:30–40.
21. Mikos AG, Temenoff JS. Formation of highly porous biodegradable scaffolds for tissue engineering. Electron J Biotechnol 2000; 3:23–24.
22. Wu C, Luo Y, Cuniberti G, Xiao Y, Gelinsky M. Three-dimensional printing of hierarchical and tough mesoporous bioactive glass scaffolds with a controllable pore architecture, excellent mechanical strength and mineralization ability. Acta Biomater 2011;7: 2644–2650.
23. Williams JM, Adewunmi A, Schek RM, Flanagan CL, Krebsbach PH, Feinberg SE, Hollister SJ, Das S. Bone tissue engineering using polycaprolactone scaffolds fabricated via selective laser sintering. Biomaterials 2005;26:4817–4827.
24. Sachlos E, Czernuszka J. Making tissue engineering scaffolds work. Review: The application of solid freeform fabrication technology to the production of tissue engineering scaffolds. Eur Cell Mater 2003;5:39–40.
25. Modaress MP, Mirzadeh H, Zandi M. Fabrication of a porous wall and higher interconnectivity scaffold comprising gelatin/chitosan via combination of salt-leaching and lyophilization methods. Iranian Polym J 2012;21:191–200.
26. Lee SB, Kim YH, Chong MS, Hong SH, Lee YM. Study of gelatin-containing artificial skin V: Fabrication of gelatin scaffolds using a salt-leaching method. Biomaterials 2005;26:1961–1968.
27. Alizadeh M, Abbasi F, Khoshfetrat A, Ghaleh H. Microstructure and characteristic properties of gelatin/chitosan scaffold prepared by a combined freeze-drying/leaching method. Mater Sci Eng C Mater Biol Appl 2013;33:3958–3967.
28. Amini AR, Adams DJ, Laurencin CT, Nukavarapu SP. Optimally porous and biomechanically compatible scaffolds for large-area bone regeneration. Tissue Eng Part A 2012;18:1376–1388.
29. Choi YS, Lee S, Hong SR, Lee Y, Song K, Park M. Studies on gelatin-based sponges. Part III: A comparative study of cross-linked gelatin/alginate, gelatin/hyaluronate and chitosan/hyaluronate sponges and their application as a wound dressing in full-thickness skin defect of rat. J Mater Sci Mater Med 2001;12:67–73.
30. Karageorgiou V, Kaplan D. Porosity of 3D biomaterial scaffolds and osteogenesis. Biomaterials 2005;26:5474–5491.
31. Holtorf HL, Datta N, Jansen JA, Mikos AG. Scaffold mesh size affects the osteoblastic differentiatioin of seeded marrow stromal cells cultured in a flow perfusion bioreactor. J Biomed Mater Res A 2005;74:171–180.
32. Takahashi Y, Tabata Y. Effect of the fiber diameter and porosity of non-woven PET fabrics on the osteogenic differentiation of mesenchymal stem cells. J Biomater Sci Polym Ed 2004;15:41–57.
33. Akay G, Birch M, Bokhari M. Microcellular polyHIPE polymer supports osteoblast growth and bone formation in vitro. Biomaterials 2004;25:3991–4000.
34. Artel A, Mehdizadeh H, Chiu YC, Brey EM, Cinar A. An agent-based model for the investigation of neovascularization within porous scaffolds. Tissue Eng Part A 2011;17:2133–2141.
35. Lewandrowski KU, Gresser JD, Bondre SP, Silva AE, Wise DL, Trantolo DJ. Developing porosity of poly(propylene glycol-co-fumaric acid) bone graft substitutes and the effect on osteointegration: A preliminary histology study in rats. J Biomater Sci Polym Ed 2000;11:879–889.
36. Cheng M, Deng J, Yang F, Gong Y, Zhao N, Zhang X. Study on physical properties and nerve cell affinity of composite films from chitosan and gelatin solutions. Biomaterials 2003;24:2871–2880.
37. Zheng JP, Wang CZ, Wang XX, Wang HY, Zhuang H, Yao KD. Preparation of biomimetic three-dimensional gelatin/montmorillonite–chitosan scaffold for tissue engineering. React Funct Polym 2007;67:780–788.
38. Thein-Han W, Saikhun J, Pholpramoo C, Misra R, Kitiyanant Y. Chitosan–gelatin scaffolds for tissue engineering: Physicochemical properties and biological response of buffalo embryonic stem cells and transfectant of GFP–Buffalo embryonic stem cells. Acta Biomater 2009;5:3453–3466.
39. Pulieri E, Chiono V, Ciardelli G, Vozzi G, Ahluwalia A, Domenici C, Vozzi F, Giusti P. Chitosan/gelatin blends for biomedical applications. J Biomed Mater Res A 2008;86:311–322.
40. Jiankang H, Dichen L, Yaxiong L, Bo Y, Hanxiang Z, Qin L, Bingheng L, Yi L. Preparation of chitosan–gelatin hybrid scaffolds with well-organized microstructures for hepatic tissue engineering. Acta Biomater 2009;5:453–461.
41. Aronow MA, Gerstenfeld LC, Owen TA, Tassinari MS, Stein GS, Lian JB. Factors that promote progressive development of the osteoblast phenotype in cultured fetal rat calvaria cells. J Cell Physiol 1990;143:213–221.
42. Huang Y, Onyeri S, Siewe M, Moshfeghian A, Madihally SV. In vitro characterization of chitosan–gelatin scaffolds for tissue engineering. Biomaterials 2005;26:7616–7627.